Optics & Laser Technology 67 (2015) 72–77

Contents lists available at ScienceDirect

Optics & Laser Technology

journal homepage: www.elsevier.com/locate/optlastec

Anti-reflection sub-wavelength structures design for InGaN-based solar cells performed by the finite-difference-time-domain (FDTD) simulation method

L.M. Yang [a], C.Y. Pan [a], F.P. Lu [a], C.W. Chang [a], S.W. Feng [b], L.W. Tu [a,c,*]

[a] Department of Physics and Center for Nanoscience and Nanotechnology, National Sun Yat-Sen University, Kaohsiung 80424, Taiwan, ROC
[b] Department of Applied Physics, National University of Kaohsiung, Kaohsiung 81148, Taiwan, ROC
[c] Department of Medical Laboratory Science and Biotechnology, Kaohsiung Medical University, Kaohsiung 80708, Taiwan, ROC

ARTICLE INFO

Article history:
Received 18 April 2014
Received in revised form
10 September 2014
Accepted 30 September 2014
Available online 23 October 2014

Keywords:
SWS array
FDTD simulation
Key parameters

ABSTRACT

The design of wide-spectrum anti-reflection (AR) sub-wavelength structures (SWS) for InGaN-based solar cells is investigated in this study. The design parameters such as base diameter and height of the SWS, as well as the pitch and fill factor of the SWS array are studied numerically in this research. The simulation is carried out by the finite-difference-time-domain (FDTD) analysis. We found that the simultaneous increase of the height of the SWS and the fill factor of the SWS array can effectively suppress the rising of the reflectance in the near-infrared range (1–2 μm). The results of the reflectance vs. wavelength for SWS array are also compared with that of the double layer anti-reflection (DLAR) coating. In addition, the effective reflectance R_{eff} which is based on AM 1.5G 1 sun considerations for various conditions is listed in Table 1 for comparison. It shows that as the height equals to 500 nm and the fill factor is greater than 0.83 (R_{eff}= 1.4%), or the fill factor equals to 1.0 and the height is greater than 200 nm (R_{eff}= 1.7%), the effective reflectance of SWS array is lower than that of DLAR coating (R_{eff}= 2.6%).

1. Introduction

The efficiency of Si-based solar cells has its limitation due to some of the inherent drawbacks such as indirect bandgap, low absorption coefficient, and so on. So far, the highest confirmed efficiency for single junction Si solar cells under the global AM 1.5G 1 sun has been around 25% [1–3]. The InGaN-based solar cells attract extensive attention nowadays mainly because their energy bandgap can be tuned from 0.65 to 3.4 eV, which covers most of the solar spectrum, by varying the indium composition [4,5]. Moreover, they have the advantages such as direct energy bandgap, high absorption coefficient, high carrier mobility, excellent radiation resistance, and so on. Due to these merits, the InGaN-based solar cells have high potential to become the next generation high-efficiency solar cells. Nevertheless, the conversion efficiency of InGaN-based solar cells has still been very low so far due to several issues such as lattice mismatch, high density of defects, phase separation, and so on [6–8].

The absorption spectrum of InGaN-based solar cells covers a wavelength ranging from ultraviolet (UV) to near-infrared (NIR) of the solar spectrum. Although the NIR region is not very significant for the Si-based solar cell because its absorption cross section is cut off at a wavelength around 1.1 μm [9,10], it is critical for the design of the configuration of InGaN-based solar cells. The effective and broadband anti-reflection (AR) design of the interface between air and the top surface of the InGaN-based solar cell can greatly improve its conversion efficiency [5,11].

For bare III–V group solar cells without any AR treatments on their top surfaces, the reflection loss can reach somewhere between 25 and 45% due to the high refractive indices of these compounds. Among various AR designs for solar cells, the dielectric thin-film coatings (DTFC) and sub-wavelength structures (SWS) are the two most frequently used methods. For DTFC, single-layer anti-reflection (SLAR) and double-layer anti-reflection (DLAR) coatings are two commonly used approaches. Although SLAR has the benefit of simplicity, it can only minimize the reflectance at certain wavelength. Multi-layer anti-reflection (MAR) coating can have better performance in the reduction of reflectance and the wavelength range of operation than both the SLAR and the DLAR. Due to the high cost and very few selections of coating materials, MAR coating is less commonly used in solar cell devices. Recently, a lot of studies have been focused on the design and fabrication of AR SWS as an AR layer on solar cells devices [11–13]. This is mainly because the SWS can effectively reduce the reflectance in a broad wavelength range by a cost-effective fabrication process [14,15].

* Corresponding author at: Department of Physics and Center for Nanoscience and Nanotechnology, National Sun Yat-Sen University, Kaohsiung 80424, Taiwan, ROC. Tel.: +886 752520003736; fax: +886 75253709.
E-mail address: lwtu@faculty.nsysu.edu.tw (L.W. Tu).

http://dx.doi.org/10.1016/j.optlastec.2014.09.016
0030-3992/

Several studies on the relations between the structural parameters of the SWS and the reflectance of the interface between air and top the surface of the solar cell have been reported [12,13,16], but less work has been done in a systematic study on this subject [17]. While most of the studies used the rigorous coupled-wave analysis (RCWA) method as a tool to do the calculations, we employed the finite-difference-time-domain (FDTD) method to do the analysis. Since the FDTD method is a very efficient and highly accurate numerical method, we can use it to do a complete and systematic study on this subject.

The aim of this paper is to investigate the key structural parameters of the wide-spectrum AR SWS design which can effectively suppress the rapid increase of the reflectance in the range of wavelength from 1 μm to 2 μm for InGaN-based solar cell. This paper is organized as follows. The FDTD simulation method is presented in Section 2. The results and discussion are given in Section 3, and the conclusion is drawn in Section 4.

2. The FDTD simulation method

The FDTD method, which was first developed by Kane Yee in 1966, is a numerical method to calculate the problems in electromagnetic. It employs a specific finite-difference discretization in solving the time-dependent Maxwell's equations. In the FDTD simulation, we focus on the relations between the reflectance and the wavelength as the parameters such as the height (h), the base diameter (b), the fill factor ($f.f.$), and the pitch (p) of the SWS array are varied.

The schematic diagram of cross sectional view of a pin double hetero-junction (HEJ) InGaN solar cell with sapphire as the substrate is shown in Fig. 1(a). The FDTD model is constructed according to this pin InGaN solar cell. The side view of this FDTD model is shown in Fig. 1(b).

2.1. Conditions and assumptions in the simulation

The thickness of non-etched layer is critical for the overall reflectance according to the previous studies on the Si_3N_4 SWS [12,13], from which it is shown that the optimum non-etched layer thickness is around 60–80 nm. Here we set the non-etched layer thickness to 70 nm. The thickness of the p-GaN layer is related to the surface recombination and the photon absorption rates. The typical thickness of p-GaN layer varies from 50 to 200 nm [18,19]. According to recent studies of Kushwaha et al. on the optimum thickness of the p-GaN layer for double hetero-junction pin solar cells, the optimum thickness is around 100 nm [18]. Here we set the thickness of p-GaN layer to 100 nm as well.

In this FDTD model, it is assumed that most of the transmitted light into the InGaN solar cell is absorbed by the pin layers (p-GaN, InGaN, and n-GaN layers) and the light reflected back to p-GaN layer can be neglected, so it is a good approximation to model the interaction between the sunlight and the InGaN solar cell with only AR SWS and the p-GaN layers as shown in Fig. 1(b). In this model, a linearly-polarized plane wave is normally incident on an array of Si_3N_4 SW parabola cone on the top of p-GaN layer. The incident wavelength ranges from 300 nm to 2000 nm in this simulation.

2.2. Comparison between the FDTD model and the Fresnel's equations

To test the accuracy and validity of the FDTD model, we compare the reflectance vs. wavelength results of the Fresnel's equations with that of the FDTD simulations for bare GaN substrate, SLAR coating, and DLAR coating. The result of this comparison is shown in Fig. 2. Here we assume that the incident linearly-polarized light is propagating in the $-Z$ direction as shown in Fig. 1(b).

The reflection from the bare GaN has only one interface between air and the GaN substrate; thus we can employ Eq. (1) below, which is derived from the Fresnel's equations to calculate

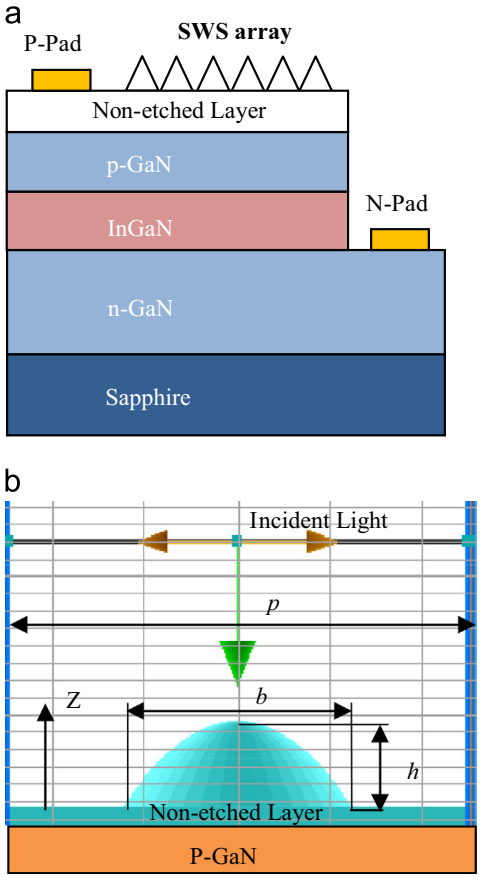

Fig. 1. The cross sectional view of InGaN solar cell: the schematic diagrams of (a) the cross sectional view of the pin double HEJ InGaN solar cell, (b) the side view of the FDTD model with the parabola cone SWS and the non-etched layer on the top of the p-GaN layer. The light is incident from $-Z$ direction.

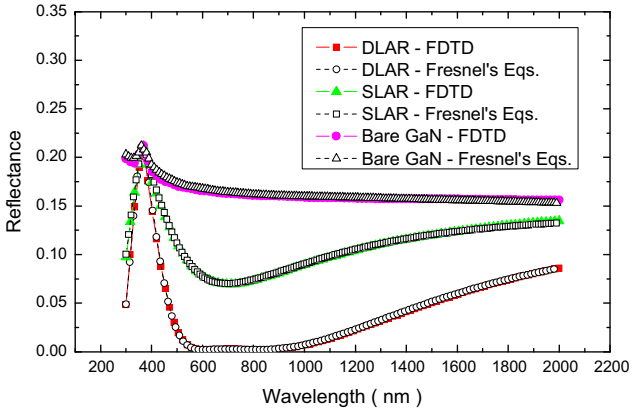

Fig. 2. The comparison of the reflectance vs. wavelength results between FDTD and Fresnel's equation for bare GaN, SLAR coating, and DLAR coating.

the reflectance as follows:

$$R = \frac{(1 - n_{G,R})^2 + n_{G,I}^2}{(1 + n_{G,R})^2 + n_{G,I}^2}, \quad (1)$$

where R is the reflectance while $n_{G,R}$ and $n_{G,I}$ are the real and imaginary parts of complex refractive index of GaN substrate n_{GaN}, respectively. That is, $n_{GaN} = n_{G,R} + i\, n_{G,I}$.

The Fresnel's equations employed to calculate the reflectance for SLAR and DLAR coatings in Fig. 2 can be expressed in transfer matrix (TM) formalism for a dielectric multi-layer system [20].

Considering a multi-layer system which has N dielectric layers and a GaN substrate, the amplitudes of the plane wave in the incident medium can be expressed as

$$\begin{pmatrix} A_0 \\ B_0 \end{pmatrix} = \begin{pmatrix} M_{11} & M_{12} \\ M_{21} & M_{22} \end{pmatrix} \begin{pmatrix} A_s \\ B_s \end{pmatrix}, \quad (2)$$

where A_0 and B_0 are the amplitudes of the plane wave propagating in $-Z$ and $+Z$ directions in the incident medium, respectively. The electric field in the incident medium can thus be expressed as $E_0(z) = A_0\, e^{i\boldsymbol{k}_{0Z}} + B_0\, e^{-i\boldsymbol{k}_{0Z}}$, where $E_0(z)$ is the electric field and $\boldsymbol{k}_0$ is the wave vector in the incident medium. Correspondingly, A_s and B_s are the amplitudes of that in the substrate medium. The transfer matrix $\boldsymbol{M}$ of this N dielectric layers system can be written as

$$\boldsymbol{M} = \begin{pmatrix} M_{11} & M_{12} \\ M_{21} & M_{22} \end{pmatrix} = D_0^{-1} \left[\prod_{l=1}^{N} D_l P_l D_l^{-1} \right] D_s, \quad l = 1, 2, \ldots, N \quad (3)$$

where D_0 and D_s are the transfer matrices for incident and substrate media, respectively. D_0^{-1} is the inverse matrix of D_0. P_l and D_l are the propagation and transfer matrices for the lth layer medium [20], respectively. The reflectance R can be expressed as

$$R = \left| \frac{M_{21}}{M_{11}} \right|^2, \quad (4)$$

where M_{21} and M_{11} are the matrix elements of transfer matrix $\boldsymbol{M}$, and can be obtained from Eq. (3) [20]. Therefore, we can obtain the reflectance for SLAR and DLAR coating systems in Fig. 2 by setting $N = 1$ and 2 in Eq. (3) for SLAR and DLAR coating systems, respectively. Then apply Eq. (4) to obtain the reflectance.

In Fig. 2, the structure of the SLAR coating is a GaN layer with 100 nm in thickness, and on top of which is a Si_3N_4 layer with 87 nm in thickness. For DLAR coating, we add an extra MgF_2 layer with 127 nm in thickness on top of the SLAR structure [21,22].

Note that on the reflectance vs. wavelength graph for the bare GaN in Fig. 2, there is a reflectance jump starting from the wavelength around 300 nm, and drops around 450 nm. This reflectance jump is due to the bandgap energy of GaN, which is at 3.4 eV. The equivalent wavelength of this absorption edge is at 365 nm, where the extinction coefficient has an increase [23,24], and so as the refractive index according to the Kramers–Kronig relations. Thus, the reflectance will increase according to Eq. (1).

3. Results and discussion

3.1. The relation between the fill factor of the SWS array and the reflectance

The fill factor (abbreviated as *f.f.*) of SWS array is defined as $f.f. \equiv b/p$, where b is the base diameter and p is the pitch of the SWS array. It can indicate the density of distribution of the SWS. We investigate two different conditions in the following. In one of them the p is fixed while the b is varied and in the other the b is fixed while the p is varied. In all figures, the result of DLAR coating which is optimized at the wavelength of 700 nm is also included for comparison.

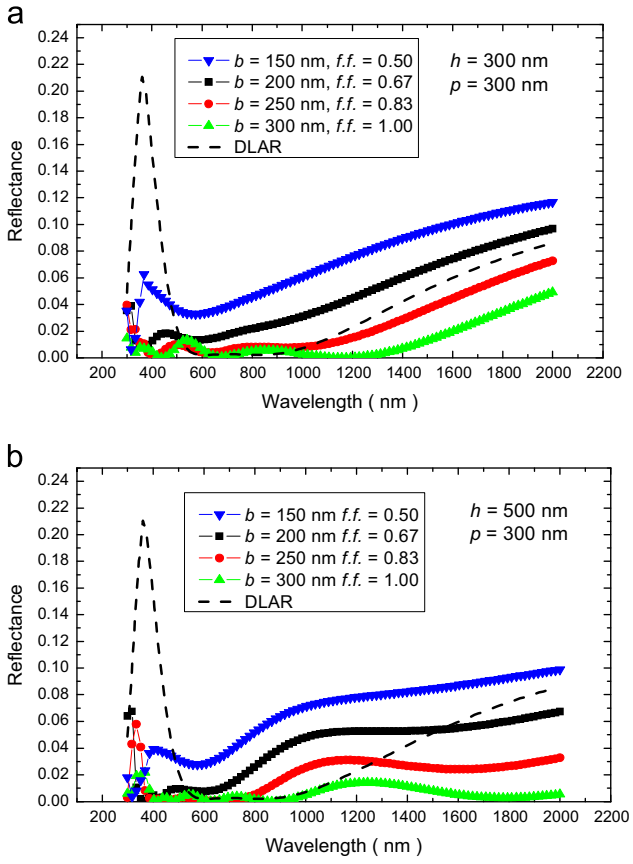

Fig. 3. The reflectance vs. wavelength for base diameter b which is varied from 150 nm, 200 nm, 250 nm , to 300 nm: (a) the height and the pitch both are kept at 300 nm, (b) the height h is fixed at 500 nm, and the pitch p remains at 300 nm.

3.1.1. The pitch is fixed while the base diameter is varied

The pitch p is fixed at 300 nm in Fig. 3(a) and (b). The height h is fixed at 300 nm in Fig. 3(a) and 500 nm in Fig. 3(b), respectively. The base diameters b are varied from 150 nm, 200 nm, 250 nm, to 300 nm, and the corresponding fill factor *f.f.* equals to 0.5, 0.67, 0.83, and 1.0, respectively.

Fig. 3(a) and (b) shows that as the base diameter b increases, the reflectance will decrease. In addition, it follows from the comparison between Fig. 3(a) and (b) that the reflectance will be more effectively suppressed as the height h is increased from 300 to 500 nm.

3.1.2. The base diameter is fixed while the pitch is varied

In Fig. 4(a) and (b), the base diameter b is fixed at 300 nm. The height h is fixed at 300 nm in Fig. 4(a) and 500 nm in Fig. 4(b). The pitch p is varied from 600 nm, 448 nm, 360 nm, down to 300 nm, and the corresponding fill factor *f.f.* equals to 0.5, 0.67, 0.83, and 1.0, respectively.

Fig. 4(a) and (b) shows that as the pitch p decreases, the reflectance will decrease as well. Moreover, the comparison between Fig. 4(a) and (b) indicates that the reflectance is more effectively suppressed as the height h is raised from 300 nm to 500 nm, especially the one for larger fill factor *f.f.*

Figs. 3 and 4 show that the reflectance slightly increases in the wavelength range of 800–1400 nm as the height h of SW parabola cones is increased from 300 nm to 500 nm. This is because the diffraction efficiency of the SW grating will increase as the height h

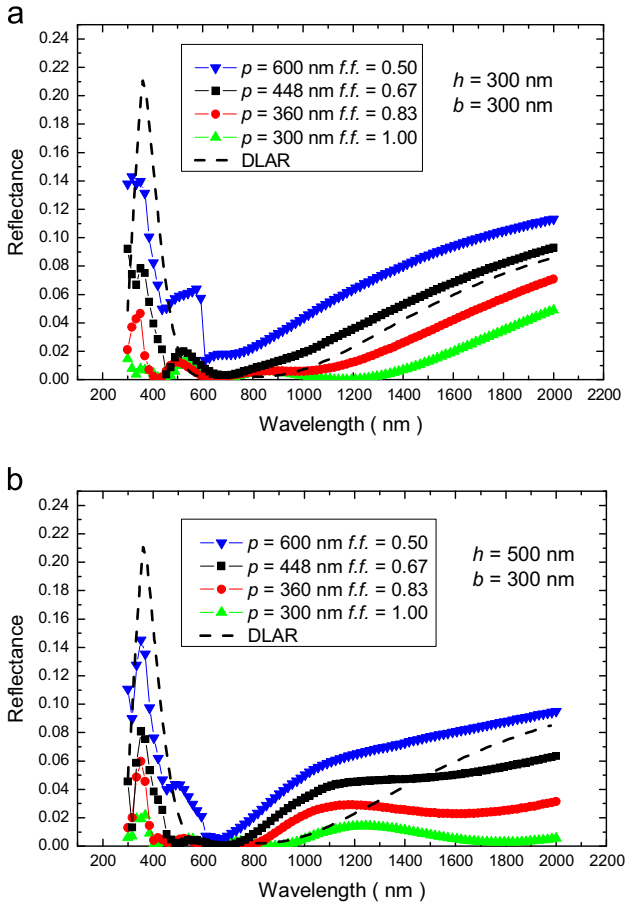

Fig. 4. Reflectance vs. wavelength for $p=600$ nm, 448 nm, 360 nm, and 300 nm, respectively: (a) the height and the base diameter both are kept at 300 nm, (b) the height h is fixed at 500 nm while the base diameter remains at 300 nm.

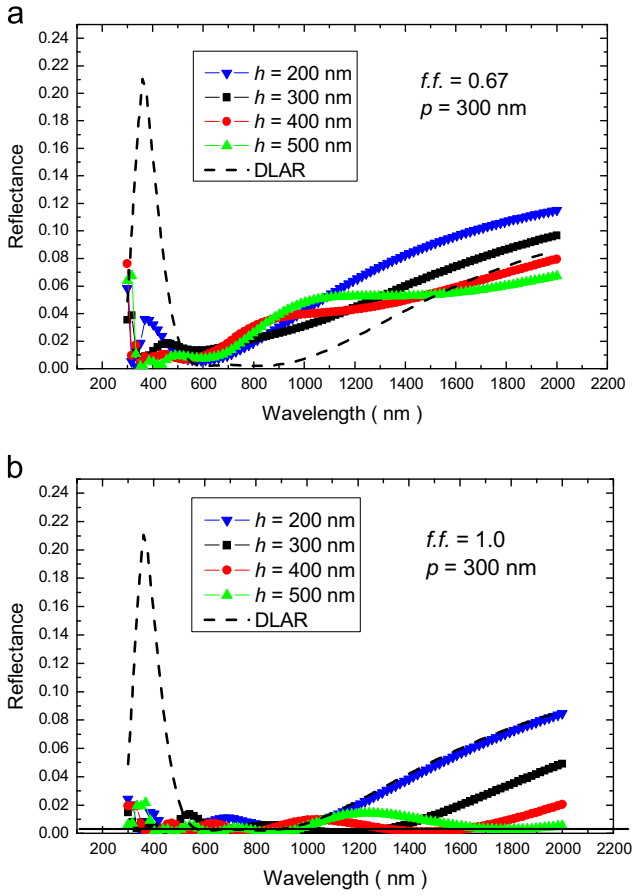

Fig. 5. The reflectance vs. wavelength for $h=200$ nm, 300 nm, 400 nm, and 500 nm: (a) the fill factor *f.f.* and the pitch p are fixed at 0.67 and 300 nm, respectively, (b) the fill factor *f.f.* and the pitch p are fixed at 1.0 and 300 nm, respectively.

of the SW parabola cones is increased, which will cause the reflection to slightly increase in this wavelength range [25]. On the other hand, in the wavelength range of 1400–2000 nm, the diffraction efficiency is less significant while EMT is more effective in this wavelength range. Thus, the reflection is effectively suppressed in the wavelength range of 1400–2000 nm as the height h is increased to 500 nm.

The AR SWS array due to its periodical structures can be treated as a 2D crossed diffraction grating. Here, we consider a one-dimensional linear diffraction grating only because a crossed diffraction grating can be treated as two perpendicular one-dimensional linear gratings.

According to the one-dimensional grating equation [26], we have

$$d(n_0 \sin\theta_0 + n\sin\theta) = m\,\lambda_0, \tag{5}$$

where d is the pitch of the grating, θ_0 and θ are the incident and the diffracted angles, respectively, n_0 and n are the refractive indices of the incident and the diffracted media, respectively, m is the diffraction order, which gives us $m=0, \pm1, \pm2, \ldots$, and λ_0 is the wavelength in vacuum. In our case here, we have $d=p=300$ nm, $\theta_0=0$ (for normal incidence), $n=n_0=1.0$ (in air), and let us set $m=1$. After we insert all these values into Eq. (5), we found that as $\lambda_0<300$ nm, the diffraction order m that can satisfy the grating equation is $m=0, \pm1$ while $\lambda_0>300$ nm, the only m that can satisfy the grating equation is $m=0$ which is a zero-order grating. Since in this study only $\lambda_0>300$ nm is considered, thus the AR SWS array is basically a zero-order grating in the simulations of this study. For a zero-order grating, all the diffracted light except zeroth order will become evanescent modes on the surface of the SWS array [27–29].

In Fig. 4(a) and (b), as the pitch $p=600$ nm, from Eq. (5) the diffraction order m can be 0 and ±1 for $\lambda_0<600$ nm. For $m=\pm1$ and $\lambda_0=300$ nm, θ is equal to $\pm30^\circ$. These two diffracted lights ($m=+1$ and -1) generate the peak in reflectance at the wavelength λ_0 around 300 nm as shown in Fig. 4(a) and (b). As the pitch p is decreased from 600 nm to 300 nm, which will transform the SWS array into a zero-order grating according to Eq. (5), the $m=\pm1$ order diffracted lights disappear. This also makes the peak at around 300 nm in wavelength disappear as shown in Fig. 4(a) and (b).

Therefore, decreasing the pitch p will increase the fill factor, which makes the distribution of the SW parabola cones denser, and helps to trap the reflected light and lower the reflectance as shown in Fig. 4(a). In addition, increasing the height h will suppress the reflectance more effectively due to the reduction of Fresnel's reflection on the SW parabola cones surfaces. The suppression of the reflectance will be more effective if the height and the fill factor are simultaneously increased as shown in Fig. 4(b).

3.2. The relation between the height of the SWS and the reflectance

In Fig. 5(a) and (b), the fill factors are fixed at 0.67 and 1.0, respectively. The pitch p is fixed at 300 nm while the height h is varied from 200 nm, 300 nm, 400 nm, to 500 nm. Fig. 5(a) shows that the reflectance can be lowered by increasing the height h. But, as shown in Fig. 5(b), it is suppressed more effectively as the fill factor is raised from 0.67 to 1.0, and especially for longer wavelength (1–2 μm).

As the height of the SW parabola cones is increased with their base diameters kept fixed, the profile of these parabola cones will become more tapered (i.e. the tapering angle is smaller), which implies that the gradient of the effective refractive index is smoother according to the effective medium theory (EMT) [12]. From the theory of Fresnel's reflection, the smoother refractive index gradient will result in less reflection. Thus, the reflectance is effectively suppressed as the height of the SW parabola cones is increased.

If only the height is raised, but the fill factor is kept low, then SW cones distribution will be too sparse to effectively trap the radiated light. It can only have little effect on reducing the reflectance as shown in Figs. 3(b), 4(b), and 5(a). Therefore, increasing the fill factor from 0.67 to 1.0 will make the distribution of SW cones denser, which can help to trap the radiated light and lower the overall reflectance as shown in Fig. 5(b).

3.3. The relations between the pitch or the base diameter of the SWS array and the reflectance

Fig. 6 shows that the reflectance vs. wavelength as the pitch p or the base diameter b of SWS array is varied from 200 nm, 230 nm, 250 nm, to 300 nm while the height h and the fill factor $f.f.$ are fixed at 500 nm and 1.0 nm, respectively.

It is shown in Fig. 6 that all the curves overlap with each other, which indicates that the reflectance only depends on the height and the fill factor, and is not directly dependent on the base diameter or the pitch of the SWS array.

The results of the reflectance are also evaluated by the effective reflectance, which can be expressed as

$$R_{eff} = \frac{\int_{\lambda_l}^{\lambda_u} R(\lambda)\, SI(\lambda) / E(\lambda)\, d\lambda}{\int_{\lambda_l}^{\lambda_u} SI(\lambda) / E(\lambda)\, d\lambda}, \tag{6}$$

where R_{eff} is the effective reflectance, $R(\lambda)$ is the wavelength dependent reflectance, $SI(\lambda)$ is the spectral irradiance given by ASTM G173 AM 1.5G reference [30], $E(\lambda)$ is the photon energy, and λ_u, and λ_l are the upper and lower bounds of the wavelength spectrum, respectively [13].

Table 1 lists the effective reflectance R_{eff}, which is calculated from Eq. (6) for various conditions of the design parameters of the AR SWS array.

In the summary of the results of Fig. 3(a) and (b) as well as Fig. 4 (a) and (b), we found that the reduction of the reflectance by either increasing the base diameter b as in Fig. 3(a) and (b) or decreasing the pitch p as in Fig. 4(a) and (b) corresponds to the increase of the fill factor $f.f.$, which is one of the dominant parameters for AR SWS design. Increasing the fill factor is equivalent to increasing the density of the SW cones distribution, which can help to trap the leaky modes or scattered light more effectively [31,32]. Moreover, increasing the height h will reduce the Fresnel's reflection on the surfaces of parabola cones. Therefore, it helps to reduce the reflectance as shown in Figs. 3(b) and 4(b).

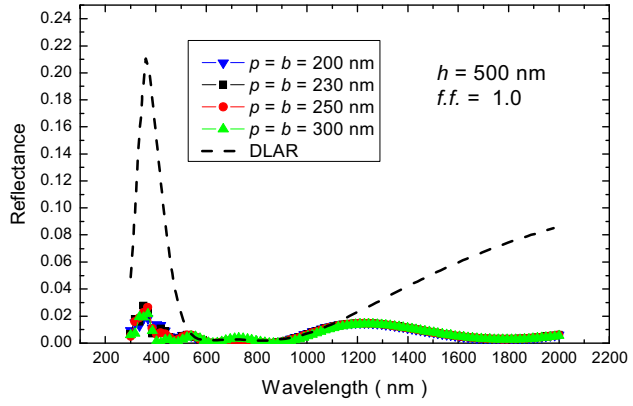

Fig. 6. The reflectance vs. wavelength for the pitch of SWS array p=200 nm, 230 nm, 250 nm, and 300 nm while the height h and fill factor $f.f.$ are fixed at 500 nm and 1.0, respectively.

Table 1
The effective reflectance for various conditions of the design parameters of AR SWS array.

Conditions for design parameters	R_{eff} (%)
p=300 nm, b=150 nm, h=300 nm ($f.f.$=0.5)	5.9
b=150 nm, h=500 nm ($f.f.$=0.5)	5.7
b=300 nm, h=500 nm ($f.f.$=1.0)	0.5
b=300 nm, p=600 nm, h=300 nm ($f.f.$=0.5)	5.2
p=600 nm, h=500 nm ($f.f.$=0.5)	4.5
p=300 nm, h=500 nm ($f.f.$=1.0)	0.5
p=300 nm, h=200 nm, $f.f.$=0.67	3.9
h=200 nm, $f.f.$=1.0	1.7
h=500 nm, $f.f.$=1.0	0.5
DLAR	2.6
$f.f.$=0.83, h=500 nm	1.4
$f.f.$=1.0, h=200 nm	1.7

From Fig. 5(a) and (b), we found that the reflectance can be lowered effectively by increasing both the height and the fill factor simultaneously especially in the wavelength region of 1–2 μm. Fig. 6 shows that the variation of either pitch or base diameter has little effect on the reflectance as long as the pitch is less than the wavelength. The height and fill factor of SWS are the two dominant factors for the design of the AR SWS array.

Table 1 shows that with the base diameter b=150 nm, the height h=300 nm, and $f.f.$=0.5, the effective reflectance is R_{eff}=5.9%. If we increase both the height and the fill factor to h=500 nm and $f.f.$=1.0, we can see that R_{eff} is reduced to 0.5%. Similarly, with p=600 nm, h=300 nm, and $f.f.$=0.5, the effective reflectance is R_{eff}=5.2%. Additionally, if we increase both the height and the fill factor to h=500 nm and $f.f.$=1.0, we can obtain the overall optimum result, and the effective reflectance is R_{eff}=0.5%. In addition, from Table 1, it shows that as long as the height h=500 nm with the fill factor $f.f.$ greater than 0.83 (R_{eff}=1.4%), or the fill factor $f.f.$=1.0 with the height h greater than 200 nm (R_{eff}=1.7%), the effective reflectance R_{eff} of SWS array is lower than that of DLAR coating (R_{eff}=2.6%).

4. Conclusions

In this paper, we studied the relations between several design parameters of SWS array and the reflectance of the AR SWS array for the InGaN-based solar cells. Among these parameters such as the height and the base diameter of SWS as well as the fill factor and the pitch of the SWS array, the height and the fill factor are the dominant ones because they can effectively suppress the increase of the reflectance in the NIR regime. Thus, they are the key parameters in the AR SWS design for InGaN-based solar cells.

According to the previous published paper of Zhang et al. [14, Fig. 7], it shows that the reflectivity decreases as the etching time of the samples increases from 3 min to 5 min for various incident angles. Since longer etching time generates deeper profiles and denser distribution of SWS, and from the experimental results above, it implies that higher SWS and larger fill factor can result in lower reflectance, which is consistent with our results.

From the results of effective reflectance in Table 1 for the AR SWS of optimum design and the DLAR coating, we found out that the former can have better anti-reflection performance than the latter in addition to its lower-cost advantage. Thus, the AR SWS approach is still an excellent candidate for anti-reflection purpose for InGaN-based solar cells as long as we control the height and the fill factor of the SWS array properly.

Acknowledgment

The authors would like to thank the company *Lumerical Solutions, Inc.* for their provision of their software *FDTD Solutions* for us to do this simulation and for their kind support as well.

References

[1] Green MA, Emery K, Hishikawa Y, Warta W, Dunlop ED. Solar cell efficiency table (version 38). Prog Photovolt: Res Appl 2011;19:562–72.
[2] Tiedje T, Yablonovitch E, Cody GD, Brooks BG. Limiting efficiency of silicon solar cells. IEEE Trans Electron Devices 1984;ED-31:711–61.
[3] Bhuiyan AG, Sugita K, Hashimoto A, Yamamoto A. InGaN solar cells: present state of the art and important challenges. IEEE J Photovolt 2012;2:276–93.
[4] Seo D-J, Shim JP, Choi SB, Seo TH, Suh E-K, Lee D-S. Efficiency improvement in InGaN-based solar cells by indium tin oxide nano dots covered with ITO films. Opt Express 2012;20:A991–6.
[5] Fu PH, Lin GJ, Ho CH, Lin CA, Kang CF, Lai YL, et al. Efficiency enhancement of InGaN multi-quantum-well solar cells via light-harvesting SiO_2 nano-honeycombs. Appl Phys Lett 2012;100:013105-1–4.
[6] Niu X, Stringfellow GB, Liu F. Phase separation in strained epitaxial InGaN islands. Appl Phys Lett 2011;99:213102-1–3.
[7] Wu YF. Investigation of strain effect in InGaN/GaN multi-quantum wells. Indian J Pure Appl Phys 2013;51:39–43.
[8] Yamaguchi S, Kariya M, Nitta S, Takeuchi T, Wetzel C, Amano H, et al. Structural properties of InN on GaN grown by metalorganic vapor-phase epitaxy. J Appl Phys 1999;85:7682–8.
[9] Mathisa SK, Romanovb AE, Chena LF, Beltzc GE, Pomped W, Specka JS. Modeling of threading dislocation reduction in growing GaN layers. J Cryst Growth 2001;231:371–90.
[10] Schubert Fred E. Light-emitting diodes. 2nd ed.Cambridge University Press; Cambridge, UK; 2006.
[11] Perl EE, Lin C-T, McMahan WE, Friedman DJ, Bowers JE. Ultrabroadband and wide-angle hybrid antireflection coatings with nanostructures. IEEE J Photovolt 2014;3:962–7.
[12] Sahoo KC, Li Y, Chang EY. Numerical calculation of the reflectance of sub-wavelength structures on silicon nitride for solar cell application. Comput Phys Commun 2009;180:1721–9.
[13] Sahoo KC, Li Y, Chang EY. Shape effect of silicon nitride subwavelength structure on reflectance for silicon solar cells. IEEE Trans Electron Devices 2010;57:2427–33.
[14] Zhang RY, Shao B, Dong RJ, Huang K, Zhao YM, Yu SZ, et al. Broadband quasi-omnidirectional antireflection AlGaInP window for III–V multi-junction solar cells through thermally dewetted Au nanotemplate. Opt Mater Express 2012;2:173–82.
[15] Miles RW, Hynes KM, Forbes I. Photovoltaic solar cells: an overview of state-of-the-art cell development and environmental issues. Prog Cryst Growth Charact Mater 2005;51:1–42.
[16] Li Y, Lee M-Y, Cheng H-W, Lu Z-L. 3D simulation of morphological effect on reflectance of Si_3N_4 subwavelength structures for silicon solar cells. Nanoscale Res Lett 2012;7:1–6.
[17] Tsai HY, Ting C-J, Kuo K-L, Chou C-P. Finite difference time domain analysis of sub-wavelength conical structured array for antireflective application. Tamkang J Sci Eng 2007;2:127–31.
[18] Kushwaha AS, Mahala P, Dhanavantri C. Optimization of p-GaN/InGaN/n-GaN double heterojunction p–i–n solar cell for high efficiency: simulation approach. Int J Photoenergy 2014:1–6.
[19] Li L, Zhao D-G, Jiang D-S, Liu Z-S, Chen P, Wu L-L, et al. The effects of InGaN layer thickness on the performance of InGaN/GaN p–i–n solar cells. Chin Phys B 2013;22:1–4.
[20] Yeh P. Optical waves in layered media. John Wiley & Sons Inc.; Hoboken, NJ; 1988; 102–14.
[21] Kavakli IG, Kantarli K. Single and double-layer antireflection coatings on silicon. Turk J Phys 2002;26:349–54.
[22] Bouhafs D, Moussi A, Chikouche A, Ruiz JM. Design and simulation of antireflection coating systems for optoelectronic devices: application to silicon solar cells. Sol Energy Mater Sol C 1998;52:79–93.
[23] Yu G, Wang G, Ishikawa H, Umeno M, Soga T, Egawa T. Optical properties of wurtzite structure GaN on sapphire around fundamental absorption edge (0.78 – 4.77 eV) by spectroscopic ellipsometry and the optical transmission method. Appl Phys Lett 1997;70:3209–11.
[24] Riedl HR, Schoolar RB. Dispersion of the refractive index near the fundamental absorption edge in PBS. Phys Rev 1963;131:2082–3.
[25] Palmer C. Diffraction grating handbook. (fifth edition). 2002; 111–5.
[26] Brown SN. Theory and simulation of subwavelength high contrast gratings and their applications in vertical-cavity surface-emitting laser devices. (Thesis for MS degree). Electrical and Computer Engineering, University of Illinois at Urbana-Champaign; Urbana, IL; 2011.
[27] Tompkin WR, Schilling A, Weiteneder C, Herzig HP. Zero-order gratings for optical variable devices. Proceedings of SPIE 2002;4677:227–37.
[28] Stork W, Streibl N, Heidner H, Kipfer P. Artificial distributed-index media fabricated by zero-order gratings. Opt Lett 1991;16:1921–3.
[29] Ding Y, Magnusson R. Band gaps and leaky-wave effects in resonant photonic-crystal waveguides. Opt Express 2007;15:680–94.
[30] Designation: G173-03 (Reapproved). Standard tables for reference solar spectral irradiance: direct normal and hemispherical on 37° tilted surface. ASTM International; West Conshohocken, PA; 2012; 1–21.
[31] Doerr CR, Kogelnik H. Dielectric waveguide theory. J Lightwave Technol 2008;26:1176–87.
[32] Marcuse D. Radiation loss of tapered dielectric slab waveguides. Bell Syst Tech J 1970;49:273–90.